

# Journal of Materials Chemistry A

Accepted Manuscript



This is an *Accepted Manuscript*, which has been through the Royal Society of Chemistry peer review process and has been accepted for publication.

*Accepted Manuscripts* are published online shortly after acceptance, before technical editing, formatting and proof reading. Using this free service, authors can make their results available to the community, in citable form, before we publish the edited article. We will replace this *Accepted Manuscript* with the edited and formatted *Advance Article* as soon as it is available.

You can find more information about *Accepted Manuscripts* in the [Information for Authors](#).

Please note that technical editing may introduce minor changes to the text and/or graphics, which may alter content. The journal's standard [Terms & Conditions](#) and the [Ethical guidelines](#) still apply. In no event shall the Royal Society of Chemistry be held responsible for any errors or omissions in this *Accepted Manuscript* or any consequences arising from the use of any information it contains.

## Sandwich-Like Cr<sub>2</sub>O<sub>3</sub>-Graphite Intercalation Composites as High-Stable Anode Materials for Lithium-ion Batteries

*Fei Wang, Wei Li, Mengyan Hou, Chao Li, Yonggang Wang and Yongyao Xia\**

Department of Chemistry and Shanghai Key Laboratory of Molecular Catalysis and Innovative Materials, Institute of New Energy, Fudan University, Shanghai 200433, China

E-mail: [yyxia@fudan.edu.cn](mailto:yyxia@fudan.edu.cn)

**Keywords:** anode material, lithium-ion batteries, Cr<sub>2</sub>O<sub>3</sub>, graphene, intercalation

### Abstract

A novel sandwich-like Cr<sub>2</sub>O<sub>3</sub>-graphite intercalation composites (Cr<sub>2</sub>O<sub>3</sub>-GICs) were synthesized via an intercalation-transformation method. Cr<sub>2</sub>O<sub>3</sub> nanoparticles (NPs) are intercalated between the adjacent carbon layers of graphite and tightly immobilized. The Cr<sub>2</sub>O<sub>3</sub>-GICs show promising performance as anode materials for LIBs with a reversible capacity of about 480 mAh/g and a relatively low lithium insertion potential. More importantly, the Cr<sub>2</sub>O<sub>3</sub>-GICs demonstrate an extremely promising stable cycling performance with over 100% capacity retention after 1000 cycles. Furthermore, the intercalation-transformation method also provides another fabrication method of graphene-based assembled materials

## Introduction

Lithium ion batteries (LIBs) have recently received much attention because of the increasing demands of power sources in electric vehicles (EV) and hybrid electric vehicles (HEV) <sup>1</sup>. Crucial components in LIBs are the electrodes, where the electrochemical reactions take place <sup>2, 3</sup>. Graphite has been commonly used as an anode material due to its good conductivity, the low volume change during the lithium insertion/extraction process, the stability of the electrode/electrolyte interphase, the low and flat operating voltage and excellent cyclability. However, its low theoretical capacity (372 mAhg<sup>-1</sup>) cannot satisfy the increasing requirements of the electronic devices and electric vehicles to the batteries.

As an alternative, metal oxides have been intensively studied as anode materials for LIBs aimed at achieving higher specific capacities than graphite over the past decades <sup>4-7</sup>. However, bulk transition-metal oxides usually suffer from a poor cycling stability due to the significant volume change and aggregation of the pulverized and/or nanosized particles, and the poor conductivity <sup>7-10</sup>. Recently, much work has been done to improve the stability and conductivity of metal oxide anodes by using carbon matrixes <sup>11-14</sup>. Graphene has emerged as an attractive alternative to other carbon allotropes because of its fascinating electronic, thermal, and mechanical properties, high specific surface areas, and easy availability from graphite <sup>15-17</sup>. To date, a variety of methods have been developed for the synthesis of metal oxide/graphene hybrid materials. However, the synthetic processes generally consist of the oxidation of graphite by strong oxidizing agents, exfoliating of graphene oxides, growth and crystallization of metal oxides, and reduction of graphene oxide sheets

<sup>18-24</sup>. The obvious drawback of these strategies is that the procedure inevitably increases the environmental imperilment, augments the preparation cost, and adds complexity to the preparation processes. On the other hand, in such formed composites, graphene are loosely stacked and the large volume changes of metal oxides upon Li insertion can only be accommodated to a limited degree, which offers only a modest improvement in cycling stability. In the attempt to overcome the capacity limitations, how to keep the low operating voltage and the good cyclability of graphite remains a big challenge.

Graphite intercalation compounds (GICs) are formed by insertion of atomic or molecular layers of different chemical species between the layers of carbon in graphite. By controlling the stage number to keep graphite occupying the major proportion, it is promising to promote the capacity to some extent without destroying the cyclability of graphite <sup>25</sup>. At the same time, appropriate lithium-ion storage intercalant can keep the low operating voltage.

Herein, we choose  $\text{Cr}_2\text{O}_3$  as intercalant for its high theoretical capacity of 1058  $\text{mAh g}^{-1}$  and relatively low lithium insertion potential among metal oxides <sup>26-30</sup>. A novel sandwich-like  $\text{Cr}_2\text{O}_3$ -graphite intercalation composites ( $\text{Cr}_2\text{O}_3$ -GICs) were synthesized via an intercalation-transformation method. In such a system,  $\text{Cr}_2\text{O}_3$  nanoparticles (NPs) are intercalated between the adjacent carbon layers and tightly immobilized, which can provide a buffer matrix for the volume change of  $\text{Cr}_2\text{O}_3$  during the charge–discharge cycling, which effectively maintains the active surface and leaves stable and open channels for ion transport. Meanwhile, the low-defect

graphene layers provide unique electrical conductivity. The  $\text{Cr}_2\text{O}_3$ -GICs show promising performance as anode materials for LIBs with low lithium insertion potential and extremely good cyclic capacity retention over 100% after 1000 cycles.

## Experimental Section

### Materials preparation

$\text{CrO}_3$ -GICs were prepared from graphite. Intercalation of  $\text{CrO}_3$  into graphite was performed according to the procedure of Platzer using a mixture of 10g graphite and 20g  $\text{CrO}_3$  in 100mL glacial acetic acid. After refluxing for 6h, the product was washed with glacial acetic acid and acetone and then dried to a constant weight.

The  $\text{Cr}_2\text{O}_3$ -GICs were prepared from  $\text{CrO}_3$ -GICs. The dried  $\text{CrO}_3$ -GICs powder were heated to 800 °C and kept for 6 hours in nitrogen atmosphere with a heating rate of 5 °C/min.

### Characterization of structure and morphology

The morphologies and particle sizes were characterized by Field-emission scanning electron microscopy (FESEM) in a Hitachi S-4800 microscope and transmission electron microscopy (TEM) on a JEOL JEM-2100 F microscope (Japan) operated at 200 kV. Thermo-Gravimetric (TG) analysis was conducted on a Mettler Toledo TGA-SDTA851 analyzer (Switzerland) from 40 to 800 °C under  $\text{O}_2$  with a heating rate of 10 °C/min. The Raman spectroscopy was conducted on a LABRAM-1B. The phase composition of the obtained  $\text{CrO}_3$ -GICs and  $\text{Cr}_2\text{O}_3$ -GICs was characterized by X-ray diffraction (XRD, Bruker D8 X-ray diffractometer) with Cu K $\alpha$  radiation.

### Measurement of electrochemical properties

The electrochemical test was carried out in CR2016-type coin cells. Metallic lithium was used as the negative electrode. The working electrodes were prepared by mixing 85% Cr<sub>2</sub>O<sub>3</sub>-GICs powders, 5% carbon black, and 10% polyvinylidene fluoride (PVDF) dissolved in *N*-methylpyrrolidinone (NMP) and the slurry mixture was then coated on Cu foil. After coating, the electrodes were dried at 80 °C for 10 min to remove the solvent before pressing. The electrodes were cut into 1 cm<sup>2</sup> sheets, vacuum-dried at 100°C for 24 h, and weighed before assembly. The typical mass loading of the active material was ~5 mg/cm<sup>2</sup>. The electrolyte solution comprised 1 M LiPF<sub>6</sub>/ethylene carbonate (EC)/diethyl carbonate (DMC)/ethyl methyl carbonate (EMC) (1:1:1 by volume). The cells were assembled with a Celgard 2300 film separator between the as-prepared cathode and lithium metal anode. Cell assembly was operated in an argon-filled glove box. Charge-discharge experiments were performed at a constant current density between 0.0 and 3.0 V using a LAND CT2001A Battery Cycler (Wuhan, China). The cells were cycled at a Lithium insertion into Cr<sub>2</sub>O<sub>3</sub>-GICs electrode referred to as discharge and extraction as charge.

### Results and discussions

**Scheme 1** illustrates the formation process of the sandwich-like Cr<sub>2</sub>O<sub>3</sub>-GICs. In a typical synthesis, CrO<sub>3</sub>-graphite intercalation composites (CrO<sub>3</sub>-GICs) were first prepared according to the procedure of Platzner using a mixture of graphite and CrO<sub>3</sub> in glacial acetic acid<sup>33</sup>. Followed by thermal annealing in N<sub>2</sub>, the intercalated molecular CrO<sub>3</sub> was transformed into uniform Cr<sub>2</sub>O<sub>3</sub> NPs, leading to the formation of

Cr<sub>2</sub>O<sub>3</sub>-GICs. In contrast to the synthesis of graphene oxide, the present reaction is not destructive with respect to the graphene structure. It should be noted that this method can only synthesize CrO<sub>3</sub>-GICs with high stage number so that the proportion of Cr<sub>2</sub>O<sub>3</sub> is relative low.

The as-obtained CrO<sub>3</sub>-GICs are micro-sized materials with a size of 10 μm (**Fig. S1**). Magnified field emission scanning electron microscopy (FESEM) images of the CrO<sub>3</sub>-GICs show a typical sandwich-like platelet structure, which indicates that graphite particles expand upon the intercalation of CrO<sub>3</sub> (**Fig. 1a**). The transmission electron microscopy (TEM) image (**Fig. 1b**) shows that the as-prepared CrO<sub>3</sub>-GICs retain the flake morphology of the graphite after the intercalation of CrO<sub>3</sub> layers. The well-defined spot patterns of selected area electron diffraction (SAED) of CrO<sub>3</sub>-GICs (**Fig. 1b**, inset) verified the single crystalline structure of graphite. Two sets of electron diffraction patterns were observed, possibly due to the displacement of graphite layers caused by the intercalation of CrO<sub>3</sub> layers. The high-magnification TEM (**Fig. 1c**) of the CrO<sub>3</sub>-GICs shows the uniform distribution of CrO<sub>3</sub> molecule between the graphite layers where no particles can be observed. The XRD (00*l*) reflection of CrO<sub>3</sub>-GICs was indexed according to the relation  $I_c = d_i + (n-1)(0.335 \text{ nm})$ , where:  $I_c$  is the unit cell repeat along the c-axis,  $d_i$  is the GIC gallery height,  $n$  is the GIC stage number, and 0.335 nm is the distance between two adjacent graphene sheets. The c-axis repeat interlayer distance of CrO<sub>3</sub>-GICs was 14.7 Å according to the X-ray diffraction (XRD) pattern (**Fig. 1d**), as expected for a stage-3 structure with CrO<sub>3</sub> molecules intercalated between tri-layer graphene planes.<sup>34</sup> The G (002) peak of

graphite almost disappeared, further suggesting the enlarging of the layer-space distance.

After the thermal annealing in  $N_2$ , the intercalated  $CrO_3$  converted to  $Cr_2O_3$  NPs. Raman technology was used to characterize the changes during the formation process of the  $Cr_2O_3$ -GICs (**Fig. 2a**). The intensity ratio of the D to G band ( $I_D/I_G$ ) is generally accepted to reflect the degree of graphitization in carbonaceous materials, and the defect density was calculated to be 0.11 for natural graphite, 0.11 for  $CrO_3$ -GICs and 0.24 for  $Cr_2O_3$ -GICs. The  $I_D/I_G$  of the  $Cr_2O_3$ -GICs increased considerably after the thermal treatment. This enhancement could be ascribed to the exfoliation of graphite and the presence of NPs between the graphite interlayer. It should be noted that the D and G band got split in  $CrO_3$ -GICs. According to the previous literature<sup>35</sup>, the Raman spectra for graphite intercalation compounds with stage  $n > 2$  (For our case,  $n = 3$ ) characteristically exhibit a doublet structure at frequencies close to the singlet  $E_{2g}$  peak found in pristine graphite. The upper frequency component of the doublet structure is identified with the graphite bounding layer mode and the lower component with the graphite interior layer mode. The above argument is strongly supported by XRD patterns of as-fabricated  $Cr_2O_3$ -GICs displayed in **Fig. 2b**. The intercalated  $Cr_2O_3$  NPs crystallized according to the Eskolaite structure with the following cell parameters:  $a = 4.9538(6) \text{ \AA}$ ,  $c = 13.585(2) \text{ \AA}$ , S.G. =  $R-3c$ . Different from that of  $CrO_3$ -GICs, the G (002) peak of graphite can be observed. After the thermal treatment, the intercalated  $CrO_3$  molecule transformed into  $Cr_2O_3$  NPs, thus the compound converted to a composite of  $Cr_2O_3$  and graphite. The repeat expanded

c- axis structure of  $\text{Cr}_2\text{O}_3$ -GICs was destroyed, as illustrated in **Scheme 1**. The repeat c-axis indexed by the XRD is the c-axis of graphite, so that the (002) peak of graphite recovered. The TGA analysis (**Fig. S2**) shows the expected low proportion of  $\text{Cr}_2\text{O}_3$  with  $\sim 16.8$  wt % in  $\text{Cr}_2\text{O}_3$ -GICs.

The sandwich-like structure of  $\text{Cr}_2\text{O}_3$ -GICs can be clearly identified based on a cross-sectional SEM image (**Fig. 3a**), which clearly reveals typical parallels and wavy layer architectures. In the regularly stacked structure,  $\text{Cr}_2\text{O}_3$  nanoparticles can be identified between the parallel layers of graphene sheets. The distortion of the planes created by the formation of  $\text{Cr}_2\text{O}_3$  nanoparticles can be clearly observed. In order to gain a much clearer knowledge of the layered sandwich structure, TEM was conducted to obtain a closer observation of the  $\text{Cr}_2\text{O}_3$ -GICs. As shown in **Fig. 3b**, particles can be observed to be distributed homogeneously with a size of about 30 nm. The SAED of  $\text{Cr}_2\text{O}_3$ -GICs (**Fig. 3b**, inset) verifies the presence of  $\text{Cr}_2\text{O}_3$  and graphite, which is consistent with the XRD result. The high-resolution TEM (HRTEM) image (**Fig. 3c**) shows that the  $\text{Cr}_2\text{O}_3$  NPs are intercalated between the graphite interlayer and tightly immobilized, which can provide a buffer matrix for the volume change of  $\text{Cr}_2\text{O}_3$  during lithiation as well as unique electrical conductivity<sup>25</sup>. It can also be indicated from the TEM image (**Fig. 3d**) that the continuous graphene layers got split due to the formation of  $\text{Cr}_2\text{O}_3$  and the emission of  $\text{O}_2$ .

The electrochemical performance of the  $\text{Cr}_2\text{O}_3$ -GICs as an anode material for LIBs was evaluated. **Fig. 4a** shows the charge/discharge curves of  $\text{Cr}_2\text{O}_3$ -GICs at a current density of 100 mA/g within the potential window of 3.0  $\sim$  0.005 V. The

Cr<sub>2</sub>O<sub>3</sub>-GICs delivered a discharge capacity of ~ 720 mAh/g and charge capacity of ~ 481 mAh/g in the first cycle, corresponding to an initial coulombic efficiency of 67 %. As found commonly in other electrode materials, the initial irreversible capacity can be ascribed to the decomposition of electrolyte during the formation of the solid electrolyte interface (SEI) film on the surface of electrode material during the first discharge, and partial irreversible decomposition of Li<sub>2</sub>O during the first charge process. However, the coulombic charge/discharge efficiency is relatively low. Because the Cr<sub>2</sub>O<sub>3</sub>-GICs are stable during the thermal treatment, we adopted the surface carbon modification method by heating the Cr<sub>2</sub>O<sub>3</sub>-GICs at 700 °C for 2h under the toluene vapour carried by nitrogen gas. After the surface modification, the initial coulombic efficiency can be improved to 86.9% (**Fig. S3**). In subsequent charge/discharge cycles, a reversible capacity of ~ 480 mAh/g was obtained. Compared to the commercial graphite anode material (~340mAh/g), the capacity of Cr<sub>2</sub>O<sub>3</sub>-GICs is 43% higher (**Fig. S4**). The theoretical capacity of Cr<sub>2</sub>O<sub>3</sub> is 1058 mAh/g, which can be calculated using the reversible electrochemical reaction: Cr<sub>2</sub>O<sub>3</sub> + 6Li=2Cr + 3Li<sub>2</sub>O<sup>29, 30, 36</sup>. For the Cr<sub>2</sub>O<sub>3</sub>-GICs, the theoretical capacity can be calculated using the following equation<sup>36</sup>:

$$C[\text{theoretical}] = C[\text{Cr}_2\text{O}_3] \times \text{wt \%}[\text{Cr}_2\text{O}_3] + C[\text{graphite}] \times \text{wt \%}[\text{graphite}].$$

According to the mass ratio of graphite to Cr<sub>2</sub>O<sub>3</sub> in Cr<sub>2</sub>O<sub>3</sub>-GICs, the theoretical capacity is 487 mAh/g, consistent with the observed capacity. It is worth noted that the lithium insertion potential of Cr<sub>2</sub>O<sub>3</sub>-GICs keeps relatively low. The discharge potential below 0.2 V shows a capacity of nearly 400 mAh/g, which is contributed

from the reduction of  $\text{Cr}_2\text{O}_3$  into  $\text{Li}_2\text{O}/\text{C}$  and the Li-ion insertion in the graphite. According to the previous report<sup>28,29</sup>, the discharge capacity of  $\text{Cr}_2\text{O}_3$  is mainly contributed from a plateau region at 0.15 V. The potential plateau could be related to the reduction of  $\text{Cr}_2\text{O}_3$  into  $\text{Li}_2\text{O}/\text{Cr}$  composite. As we all know, the potential for the conventional Li-ion insertion reaction in the natural interlayer of graphite is also below 0.2V. The low lithium insertion potential is also convinced by the cyclic voltammogram result (**Fig. S5**). **Fig. S5** shows the cyclic voltammogram of the  $\text{Cr}_2\text{O}_3$ -GICs electrodes for the initial 2 cycles. The broad cathodic peaks at 0.69 V in the first cycle, which can be attributed to the formation of the SEI film on the surface of the anode, disappear from the second cycle. Once the SEI layer forms, a new SEI layer does not form under subsequent process of Li-ion insertion and extraction. The anodic peak at 0.27 V observed from the first scan cycle corresponds to the extraction of Li-ions from the  $\text{Cr}_2\text{O}_3$ -GICs. The anodic peaks are still distinct and stable during the subsequent cycles.

Besides the high capacity and low lithium insertion potential,  $\text{Cr}_2\text{O}_3$ -GICs electrodes also show excellent cycling stability, as displayed in **Fig. 4b**. The electrode provides a capacity of about 420 mAh/g with a little capacity loss after 200 cycles. The reversible capacity increased to 520 mAh/g after 1000cycles (at a current density of 100 mA/g), demonstrating an extremely promising stable cycling performance over a prolonged testing period. **Fig. S6** shows the cyclability of the  $\text{Cr}_2\text{O}_3$ -GICs electrodes at 10 C after the first 100 cycles at 0.2 C (100 mA/g as 0.2C). The specific reversible capacity after 2000 cycles is 140 mAh/g at 10 C. The  $\text{Cr}_2\text{O}_3$ -GICs electrodes also

exhibit good capacity retention in high rate. After 2000 cycles, the  $\text{Cr}_2\text{O}_3$ -GICs electrode could sustain 100% capacity of the 101th cycle at 10 C. When the rate is lowered to 0.2 C again, the reversible capacity of 560mAh/g is regained, demonstrating the excellent reversibility. The possible reasons for the capacity increment were the reversible growth of the polymeric gel-like film due to the kinetically activated electrolyte degradation and the exfoliation and lattice damage caused by the intercalation/de-intercalation of Li ions, which short the movement distance of Li ions in the spatially packed graphene layers. The Li-ion adsorption/desorption on the surface of graphene sheet both sides of  $\text{Cr}_2\text{O}_3$  intercalated layer may also cause the excess capacity. In contrast, control electrodes fabricated by directly mixing  $\text{Cr}_2\text{O}_3$  nanoparticles with graphite showed significantly lower stability (**Fig. S7**) due to the loss of electrical pathway. The outstanding cycle performance of  $\text{Cr}_2\text{O}_3$ -GICs can be attributed to its unique structure. Firstly, the regularly stacked structure, where electrochemically active species are sandwiched between graphene interlayer, provides a buffer matrix for the volume change of  $\text{Cr}_2\text{O}_3$  during lithiation. Secondly, the graphene layer provides unique electrical conductivity, and thirdly, the presence of  $\text{Cr}_2\text{O}_3$  distributed in the interlayer space expands the distance between the graphene layers which allows rapid diffusion of lithium ions in and out of the material.

To investigate why the  $\text{Cr}_2\text{O}_3$ -GICs show an outstanding excellent electrochemical performance, the TEM images of  $\text{Cr}_2\text{O}_3$ -GICs in the charge state after the 1000th cycle were investigated. Even after the prolonged testing period,  $\text{Cr}_2\text{O}_3$

NPs can still be observed to be distributed homogeneously with no aggregation or structure collapse, as shown in **Fig. 5a**. **Fig. 5b** shows that the  $\text{Cr}_2\text{O}_3$  nanoparticles are immobilized between adjacent layers. Though the  $\text{Cr}_2\text{O}_3$  became amorphous after the long term cycle, which can be confirmed by the XRD results (**Fig. S8**), the amorphous particles still keep tight contact with others in the immobilized area to keep the origin particle morphology. The unique structure of GICs appears to effectively solve the bottleneck problem of preventing capacity loss due to large volume change. The  $\text{Cr}_2\text{O}_3$ -GIC still keep the tightly stacked structure and the graphene layer plays a very important role in stabilization of  $\text{Cr}_2\text{O}_3$  particles. Being different from the previous carbon modification technology in which the carbon layer in the carbon coated or core-shell structure will be destroyed during long cycling, the graphene layers in our case provide a very stable buffer matrix for the volume change during lithiation. The graphene layers have good elasticity to effectively accommodate the strain of volume change during  $\text{Li}^+$  insertion/extraction. Moreover, the graphene layers always keep tight contact with the  $\text{Cr}_2\text{O}_3$  particles even after a long term cycle, which is important to improve the cycle performance.

## Conclusions

In conclusion, we reported the synthesis of  $\text{Cr}_2\text{O}_3$ -GICs by intercalating the  $\text{CrO}_3$  into the graphite interlayer followed by the thermal treatment. In this case, the  $\text{Cr}_2\text{O}_3$ -GICs were obtained without the oxidation of graphite. The resultant  $\text{Cr}_2\text{O}_3$ -GICs has a reversible capacity as large as 500 mAh/g and a relatively low lithium insertion potential. More importantly, the  $\text{Cr}_2\text{O}_3$ -GICs demonstrate an

extremely promising stable cycling performance with over 100% capacity retention after 1000 cycles. We believe that the graphite intercalation composite provides a most facility way to improve the capacity of graphite anode without affecting the low working potential. Furthermore, the intercalation-transformation method also provides another fabrication method of graphene-based assembled materials compared with the complex conventional assembly process, which typically involves oxidation, exfoliating, assembly and reduction etc. Both the synthesis and the structure design strategies might also be extended to other anode materials for lithium-ion batteries.

#### **Acknowledgements**

(This work was partially supported by the National Natural Science Foundation of China (No.20925312), the State Key Basic Research Program of PRC (2011CB935903), and Shanghai Science & Technology Committee (08DZ2270500).

#### **Appendix A. Supplementary materials**

Supplementary data associated with this article can be found in the online version at

#### **References**

- [1] M. Armand, J.M. Tarascon, *Nature*, 2008, **451**, 652.
- [2] I. Kovalenko, B. Zdyrko, A. Magasinski, B.Hertzberg, Z. Milicev, R. Burtovyy, I. Luzinov, G. Yushin, *Science*, 2011,**333**, 75.
- [3] A. Magasinski, P. Dixon, B. Hertzberg, A. Kvit, J. Ayala, G. Yushin, *Nat. Mater.*, 2010, **9**, 353.
- [4] P. Poizot, S. Laruelle, S. Grugeon, L.Dupont, J.M. Tarascon *Nature*, 2000, **407**, 496.

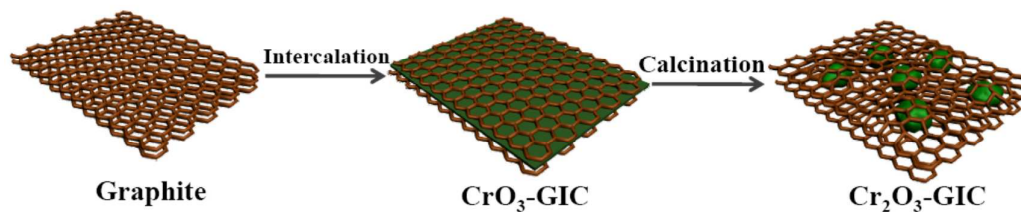
- [5] L. Taberna, S. Mitra, P. Poizot, P. Simon, J.M. Tarascon, *Nat. Mater.*, 2006, **5**, 567.
- [6] M. Morcrette, P. Rozier, L. Dupont, E. Mugnier, L. Sannier, J. Galy, J.M. Tarascon, *Nat. Mater.*, 2003, **2**, 755.
- [7] Y. Ren, L.J. Hardwick, Bruce, P. G. *Angew. Chem. Int. Ed.*, 2010, **49**, 2570.
- [8] X.W. Lou, Y. Wang, C.L. Yuan, J.Y. Lee, L.A. Archer, *Adv. Mater.*, 2006, **18**, 2325.
- [9] Z.Y. Wang, L. Zhou, X.W. Lou, *Adv. Mater.*, 2012, **24**, 1903.
- [10] W. Li, F. Wang, S.S. Feng, J.X. Wang, Z.K. Sun, B. Lin, Y.H. Li, J.P. Yang, A.A. Elzatanhry, Y.Y. Xia, D.Y. Zhao, *J. Am. Chem. Soc.*, 2013, **135**, 18309.
- [11] Y.M. Chiang, *Science*, 2010, **330**, 1485.
- [12] P.G. Bruce, B. Scrosati, J.M. Tarascon, *Angew. Chem. Int. Ed.*, 2008, **47**, 930.
- [13] L.W. Ji, Z. Lin. M. Alcoutlabi, X.W. Zhang, *Energy Environ. Sci.*, 2011, **4**, 2682.
- [14] F. Li, Q.Q. Zou, Y.Y. Xia, *J. Power Sources*, 2008, **177**, 546.
- [15] S. Stankovich, D.A. Dikin, G.H.B. Dommett, K.M. Kohlhaas, E.J. Zimney, E.A. Stach, R.D. Piner, S.T. Nguyen, R.S. Ruoff, *Nature*, 2006, **442**, 282
- [16] Q.J. Xiang, J.G. Yu, M. Jaroniec, *Chem. Soc. Rev.*, 2012, **41**, 782
- [17] S. Yang, R.E. Bachman, X. Feng, K. Müllen, *Accounts. Chem. Res.* 2012, **46**, 116.
- [18] Z. Liu, J.T. Robinson, X.M. Sun, H.J. Dai, *J. Am. Chem. Soc.*, 2008, **130**, 10876
- [19] H.L. Wang, L.F. Cui, Y.A. Yang, H.S. Casalongue, J.T. Robinson, Y.Y. Liang, Y. Cui, H.J. Dai, *J. Am. Chem. Soc.*, 2010, **132**, 13978
- [20] F. Wang, J. Yi, Y.G. Wang, Y.Y. Xia, *Nanotechnology*, 2013, **24**, 424010

- [21] S.B. Yang, X.L. Feng, X.C. Wang, K. Mullen, *Angew, Chem. Int. Ed.*, 2011, 50, 5339
- [22] Z.S Wu, S.B. Yang, Y. Sun, K. Parvez, X.L. Feng, K. Mullen, *J. Am. Chem. Soc.*, 2012, **134**, 9082
- [23] J. Liang, Y. Jiao, M. Jaroniec, S.Z. Qiao, *Angew, Chem. Int. Ed.*, 2012, **51**, 11496
- [24] S.M. Paek, E. Yoo, I.Honma, *Nano Lett.*, 2009, **9**, 72
- [25] F. Wang, J. Yi, Y.G. Wang, C.X.Wang, J.Q.Wang, Y.Y. Xia, *Adv. Energy Mater.*, 2014, **4**, 1300600
- [26] S. Grugeon, S. Laruelle, L. Dupont, F. Chevallier, P.L. Taberna, P. Simon, L.Gireaud, S. Lascaud, E. Vidal, B. Yrieix, J.M. Tarascon, *Chem. Mater.*, 2005, **17**, 5041.
- [27] H. Li, P. Balaya, J. Maier, *J. Electrochem. Soc.*, 2004, **151**, A1878.
- [28] J. Hu, H. Li, X.J. Huang, L.Q. Chen, *Solid State Ionics*, 2006, **177**, 2791.
- [29] J. Hu, H. Li, X.J. Huang, *Electrochem.Solid-State Lett.*, 2005, **8**, A66.
- [30] L.Y. Jiang, S. Xin, X.L. Wu, H. Li, Y.G. Guo, L.J. Wan, *J. Mater. Chem.*, 2010, 20, 7565
- [31] K.P. Loh, Q.L. Bao, G. Eda, M. Chhowalla, *Nature Chem.*, 2010, 2, 1015.
- [32] C. Gómez-Navarro, J.C. Meyer, R.S. Sundaram, A. Chuvilin, S. Kurasch, M. Burghard, K. Kern, U. Kaiser, *Nano Lett.*, 2010, **10**, 1144
- [33] N. Platzer, B. Martiniere, *Bull. Soc. Chim. Fr.*, 1961, **197**
- [34] J.M. Skowronski, *Synthetic Metals.*, 1995, **73**, 21.
- [35] M.S.Dresselhaus, G.Dresselhaus, *Advances in Physics*, 2002, **51**, 1.

[36] G.X.Zhao, T.Wen, J. Zhang, J.X. Li, H.L. Dong, X.K. Wang, Y.G. Guo, W.P.

Hu, *J. Mater. Chem.*, 2014, **5**, 944

## Figures and Caption



**Scheme 1.** Schematic illustration of the formation process of the  $\text{Cr}_2\text{O}_3\text{-GICs}$ .

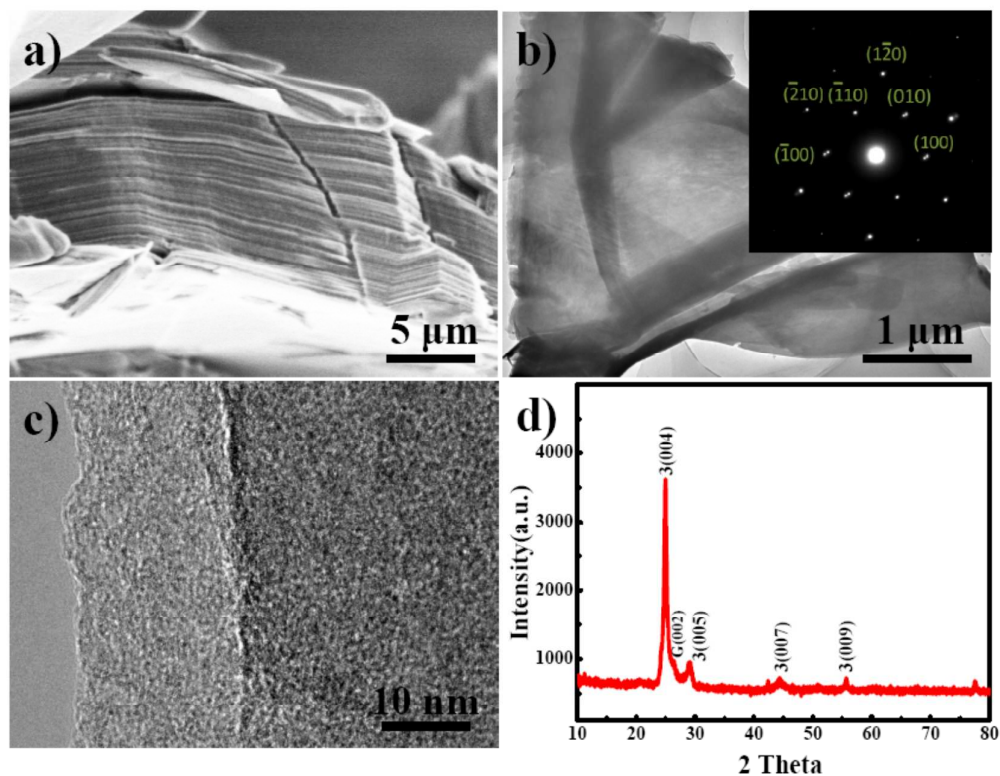


**Figure 1.** Characterization of  $\text{CrO}_3\text{-GIC}$ : a) FESEM images; b) TEM image (inset the electron diffraction pattern) c) HRTEM image; d) the powder X-ray diffraction (XRD) data.

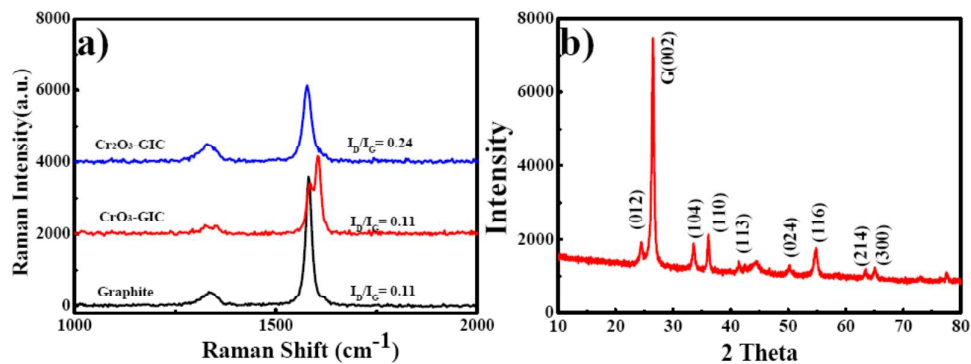


**Figure 2** a) Raman spectra of natural graphite, CrO<sub>3</sub>-GICs, and Cr<sub>2</sub>O<sub>3</sub>-GICs. b) X-ray patterns of the Cr<sub>2</sub>O<sub>3</sub>-GICs;

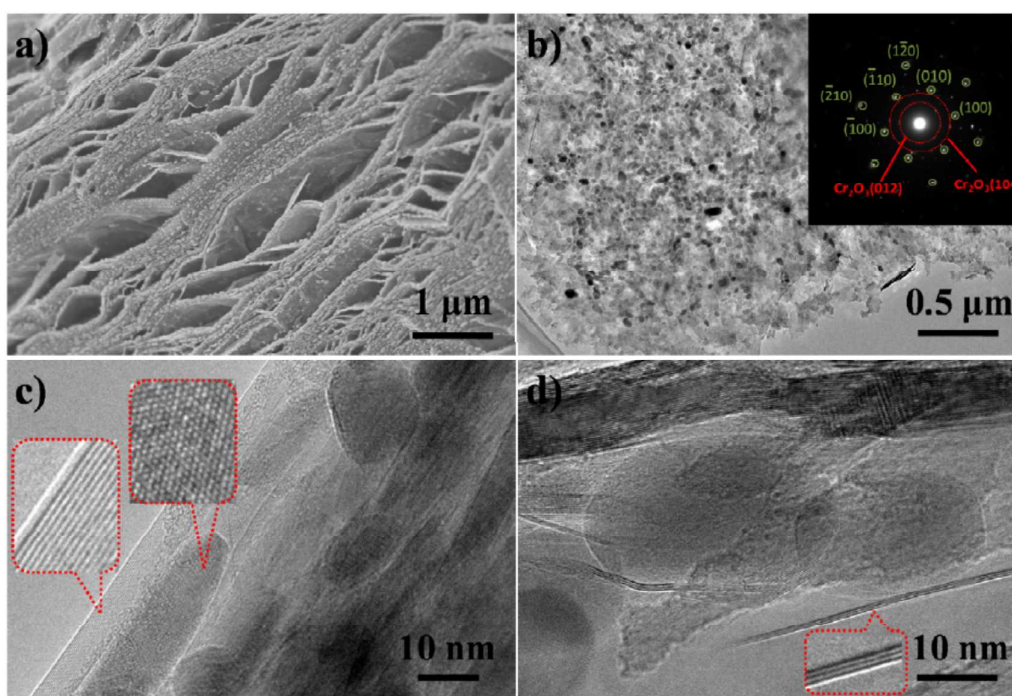


**Figure 3** Characterization of Cr<sub>2</sub>O<sub>3</sub>-GICs: a) FESEM image b) TEM image (inset the electron diffraction pattern); c) HRTEM image d) HRTEM image.

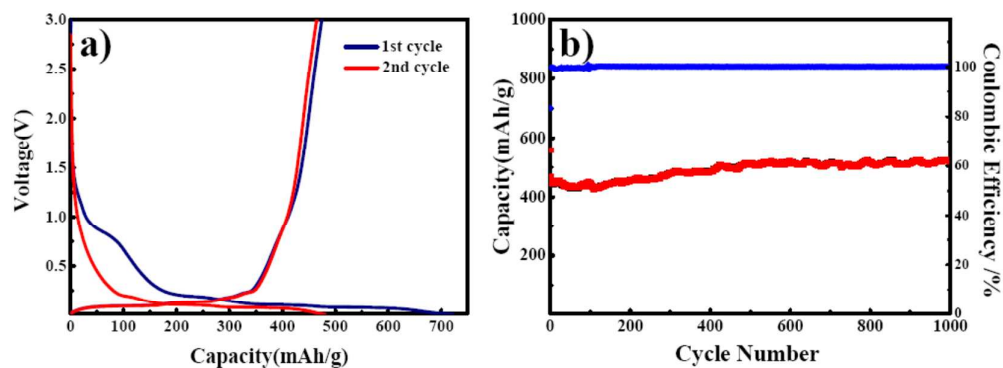


**Figure 4** a) Charge/discharge curves of  $\text{Cr}_2\text{O}_3$ -GICs between voltage limits of 0 and 3.0 V at a current of 100 mA/g; b) cycle ability of  $\text{Cr}_2\text{O}_3$ -GICs between voltage limits of 0 and 3.0 V at a current of 100 mA/g at room temperature.

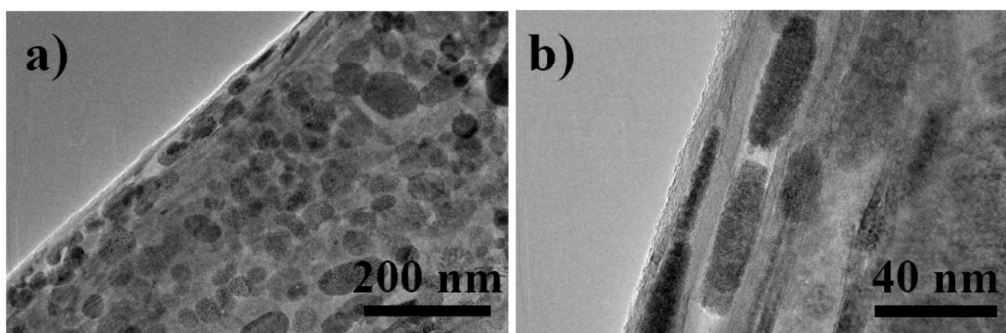


**Figure 5.** TEM images of the  $\text{Cr}_2\text{O}_3$ -GICs after 1000 discharge-charge cycles

